On the Choice of Coil Combination Weights for Phase-Sensitive GRAPPA Reconstruction in Multichannel SWI

Sreekanth Madhusoodhanan and Joseph Suresh Paul

Abstract The feasibility of applying Generalized Auto-calibrating Partially Parallel Acquisition (GRAPPA) techniques has been established, with a two-fold or more reduction in scan time without compromising vascular contrast in Susceptibility Weighted Imaging (SWI) by choosing an optimal sensitivity map for combining the coil images. The overall SNR performance in GRAPPA is also dependent on the weights used for combining the GRAPPA reconstructed coil images. In this article, different methods for estimating the optimal coil combination weights are qualitatively and quantitatively analysed for maximizing the structural information in the tissue phase. The performance of various methods is visually evaluated using minimum Intensity Projection (mIP), Among the three methods, sensitivity estimated using the dominant eigenvector mentioned as ESPIRiT-based sensitivity in this article shows superior performance over the other two methods including estimating the sensitivity from the centre k-space line and from reconstructed channel images. Combining channel images using ESPIRiT sensitivity shows its ability to preserve the local phase variation and reduction in noise amplification.

Keywords Coil combination · Parallel imaging · Sensitivity · SWI

1 Introduction

Susceptibility Weighted Imaging (SWI) is an MR imaging technique which utilizes the susceptibility variations between tissues in human body to image them [1–8]. These variations in the susceptibility of tissues are embedded in the phase of the MR image [1, 9]. The acquisition parameters are so chosen such that sufficient susceptibility contrast was obtained from vessels while simultaneously reducing

S. Madhusoodhanan (✉) · J. S. Paul
Medical Image Computing and Signal Processing Group, Indian Institute of Information Technology and Management-Kerala (IIITM-K), Trivandrum, Kerala, India
e-mail: sreekanth.m@iiitmk.ac.in

J. S. Paul
e-mail: j.paul@iiitmk.ac.in

B. B. Chaudhuri et al. (eds.), *Proceedings of 3rd International Conference on Computer Vision and Image Processing*, Advances in Intelligent Systems and Computing 1022,
https://doi.org/10.1007/978-981-32-9088-4_10

contrast among white matter, grey matter and ventricles [10]. As a result, the total acquisition time for SWI remains long. This results in motion-induced artefacts and patient discomfort. Thus, there is a need for faster acquisition time and efficient ways of combining multichannel coil data without losing the phase information.

Partially Parallel Imaging (PPI) acquisitions and reconstruction algorithms have been used commonly in clinical applications to speed up the MR acquisition without significantly reducing the Signal-Noise-Ratio (SNR) and contrast between vessels and other brain regions. SENSitivity Encoding (SENSE) [11] is an image domain based parallel imaging method which is highly subjected to B0 and B1 field inhomogeneity. Auto-calibrating techniques such as GeneRalized Auto-calibrating Partially Parallel Acquisitions (GRAPPA) can better handle the field inhomogeneities because GRAPPA reconstruction makes use of the fully sampled centre k-space data known as the auto-calibrating lines, whereas SENSE relies on coil sensitivity maps to estimate the unaliased image [12, 13]. Recent work has demonstrated the application of auto-calibrated data-driven parallel imaging methods to phase-sensitive imaging without any apparent impact on image phase. Lupo et al. [14] have demonstrated that GRAPPA reconstruction shows improved vessel contrast as compared to SENSE when applied to SWI Brain vasculature data acquired at 7T with reduction factor ($R = 2$).

The feasibility of accelerating SWI acquisitions by using parallel imaging techniques has shown that GRAPPA has an advantage over SENSE in terms of robustness in detecting small vessels [14]. In this work, GRAPPA reconstruction is applied on undersampled SWI images, which are then coil combined using three different types of coil combination weights suggested in the literature [15, 16]. The quality of phase-sensitive reconstruction is assessed by the application of venous enhancement filtering on the final combined image obtained using each coil combination weights.

2 Materials and Methods

2.1 Data Acquisition

Dataset-1: SWI is collected from volunteers using a Siemens 1.5T scanner with uniform excitation by a volume transmitter and reception by 32-channel head array coil. TE/TR values were 40/49 ms with a nominal flip angle (FA) of 20° and slice thickness 2.1 mm. The collected data was retrospectively undersampled by a factor of three prior to performing GRAPPA. The number of auto-calibrating (nACS) lines used is 24; Field of view (FOV) = 203 × 250 mm and the reconstructed matrix size is 260 × 320.

Dataset-2: SWI data is from a patient with multiple micro haemorrhages seen in the cerebellum and left temporal lobe. The acquisition was performed with a Siemens 1.5T scanner using 32 channel head array coils. The scan parameters were TE = 40 ms, TR = 49 ms, FA = 20°, slice thickness 2.1 mm, FOV = 203 × 250 and the reconstructed matrix size is 260 × 320.

Dataset-3: Multi-echo SWAN data was acquired on GE 3T MRI system equipped with a 12-channel head array coil using a three-dimensional gradient echo sequence. Scan parameters were as follows: repetition time (TR) = 42.6 ms, TE = 24.7 ms, flip angle (FA) = 15°, slice thickness of 2.4 mm acquisition matrix of 384 × 288, bandwidth (BW) = 325.52 Hz/pixel and FOV = 260 × 260 mm.

2.2 Reconstruction and Post-processing of Complex Multichannel Data

SWI data was acquired and retrospectively undersampled by an acceleration factor (R) while retaining central Auto-Calibrating Signal (ACS) lines. The GRAPPA-based parallel imaging technique employed a two-dimensional 2 × 7 interpolation kernel using two neighbouring points in the Phase Encode (PE) direction, placed symmetrically around the missing line and seven neighbouring data points in the Frequency Encode (FE) axis. After reconstruction, various post-processing techniques were employed as shown in Fig. 1 to obtain the final image.

2.3 GRAPPA Reconstruction

GRAPPA is a parallel MRI technique to estimate the missing k-space points by linearly combining more than one acquired line. GRAPPA uses the fully sampled centre k-space region (ACS lines) of each channel for training to estimate the unacquired data. Using a linear combination of the acquired PE lines and GRAPPA weights computed from ACS data, the unacquired points are estimated. The calibration step for GRAPPA weight calculation and estimation of unacquired points in the outer k-space are the two main steps in the reconstruction procedure. Calibration is performed using samples from ACS lines, forming the training data. Let k_{y} be the index of the acquired line in the phase encode direction, then the target data $\mathrm{K}^{l}(k_{\mathrm{y}} + \eta\Delta k_{\mathrm{y}}, k_{\mathrm{x}})$ in the basic GRAPPA model with acceleration factor R and η varies from 1 to R−1, which can be defined from the source data $\mathbf{k}(k_y, k_x)$ at the location (k_y, k_x) as,

$$K^{l}(k_y + \eta\Delta k_y, k_x) = \mathbf{z}_{\eta}^{l}\mathbf{k}(k_y, k_x) \tag{1}$$

where $\mathbf{k}(k_y, k_x)$ represents a collection of acquired neighbouring samples for a particular location from all coils and $\mathbf{z}_{\eta}^{l}$ is the GRAPPA weights. For all training pairs in ACS $\{\mathbf{k}(k_y, k_x), K^{l}(k_y + \eta\Delta k_y, k_x)\}$ represented the calibration weights $\mathbf{z}_{\eta}^{l}$ are first estimated by inversion of (1). Though all locations within ACS are truly acquired, k_{y} refers to only those locations that strictly follow the sampling pattern in the outer k-space. The calibration matrix Π is now obtained by row-wise appending of the training set $\mathbf{k}(k_y, k_x)$ corresponding to each acquired ACS location following the

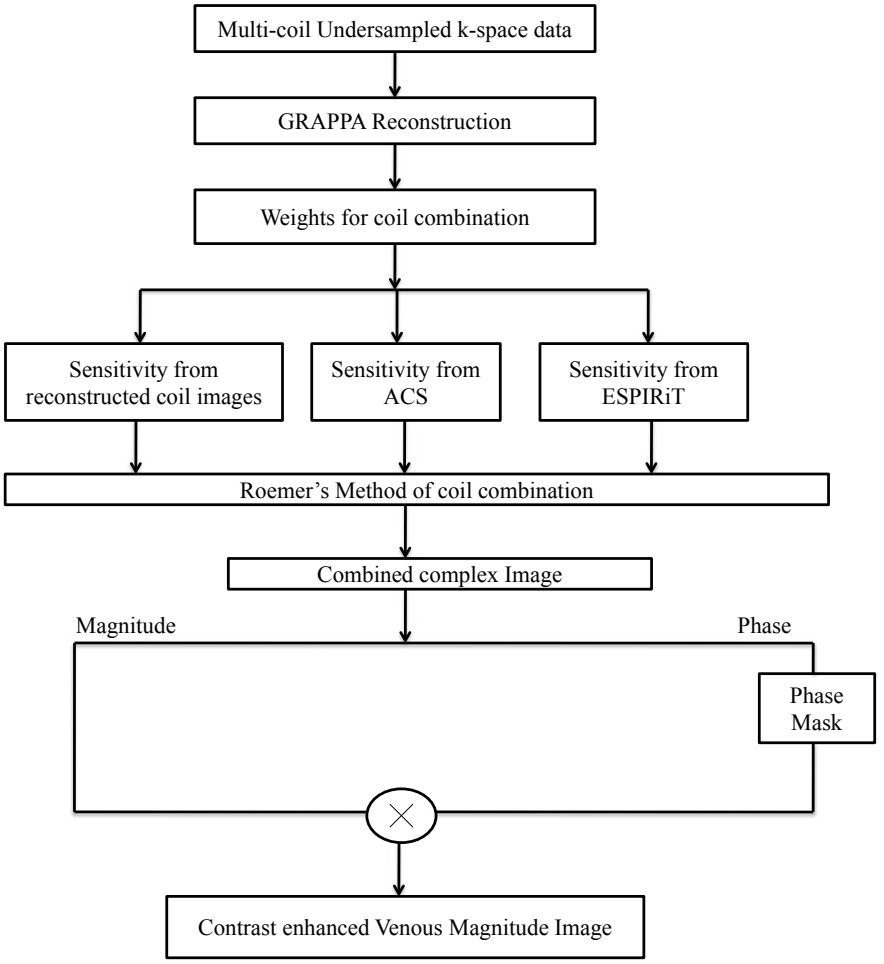

Fig. 1 Work flow showing venous enhancement

sampling pattern. The observation vector $\mathbf{k}_u$ for calibration is obtained from each training pair by considering the elements $K^l\left(k_y + \eta\Delta k_y, k_x\right)$. By determining the least squares (LS) solution, the calibration process is defined as

$$\mathbf{z}_\eta^l = \left(\Pi^{\mathrm{H}}\Pi\right)^{-1}\Pi^{\mathrm{H}}\mathbf{k}_u \tag{2}$$

Missing k-space value $\mathrm{K}^l\left(k_y + \eta\Delta k_y, k_x\right)$ in the outer k-space is estimated by applying the filter obtained from calibration z_η^l to the acquired dataset $\mathbf{k}\left(k_y, k_x\right)$. In GRAPPA reconstruction, the unacquired points in the sample k-space for *j*th coil is estimated as

$$\mathrm{K}^{j}\left(k_x, k_y + \eta\Delta k_y\right) = \sum_{l=1}^{n_c} \sum_{b=-P_l}^{P_k} \sum_{h=-F_l}^{F_k} K^{l}\left(k_y + bR\Delta k_y, k_x + h\Delta k_x\right) z_{\eta}^{l} \quad (3)$$

where h and b denote sampling indices along the frequency and phase-encoding directions, respectively.

2.4 Methods for Coil Combination

Roemer et al. demonstrated an optimal way to combine the data from multiple channels using an estimated or true sensitivity profile [15]. The combined complex image ($\mathrm{I_R}$) is obtained as

$$\mathrm{I_R} = \frac{\sum_{k=1}^{n_c} P_k^{*} S_k}{\sum_{k=1}^{n_c} |P_k|^2} \quad (4)$$

Sensitivity estimate from coil images. After estimation of unacquired points using GRAPPA reconstruction, the k-space data is inverse Fourier transformed to obtain the channel images. Absolute value of each coil image is divided by root-Sum-of-Squares (rSoS) image to estimate the coil sensitivity map from the reconstructed channel image.

Sensitivity from ACS. One of the most common ways of obtaining the sensitivity is from the Auto-Calibrating lines (ACS) of the undersampled k-space. The central ACS data (e.g. 24 × 24) is zero-padded to the size of the image and inverse Fourier transformed to obtain the low-resolution sensitivity map.

ESPIRiT-based sensitivity estimation. This procedure for estimating the coil sensitivity has evolved from efficient eigenvector-based implementation in the calibration steps of the original SPIRiT approach and its parallel imaging implementation is referred to as ESPIRiT [16]. In ESPIRiT, the calibration matrix is first decomposed using Singular Value Decomposition (SVD) into a left singular matrix U, a right singular matrix V and a diagonal matrix S of singular values [10]. The basis for the rows of the calibration matrix Π is obtained from the columns of the V matrix in the SVD of calibration data. The matrix V is then separated into V⊥ which spans the null space of Π and V. In ESPIRiT, the calibration matrix is first decomposed using Singular Value Decomposition (SVD) into a left singular matrix U, a right singular matrix V and a diagonal matrix S of singular values [17]. The basis for the rows of the calibration matrix Π is obtained from the columns of the V matrix in the SVD of calibration data. The matrix V is then separated into V⊥ which spans the null space of Π and V‖ which spans its row space. In ESPIRiT, the coil combination weights are derived from the dominant eigenvectors of the subspace spanned by the row space of

Π. Similarly, these weights from dominant eigenvectors can be used for combining the channel images after GRAPPA reconstruction, which spans its row space.

2.5 *Homodyne Filtering*

Homodyne filter is a type of high-pass filter which is widely used to remove the phase variations due to main field inhomogeneities and air-tissue interface. In Susceptibility imaging, the tissue susceptibility effects are local and exist primarily in high spatial frequencies, while external field effects exist primarily in the low spatial frequencies [18]. The high-pass filter is obtained by taking the original image $\rho(r)$, truncating it to the central complex image $\rho_n(r)$, creating an image by zero filling the elements outside the central elements and then complex dividing $\rho(r)$ by $\rho_n(r)$ to obtain a new image.

$$\rho'(r) = \rho(r)/\rho_n(r) \tag{5}$$

The phase masks scaled between 0 and 1 are designed to enhance the contrast in the original magnitude image by suppressing pixels having certain phase values. The venous enhanced image is obtained by element-by-element multiplication of the original magnitude image with the phase mask. Usually, the phase mask is multiplied 'r' times to increase the susceptibility-related contrast. In this article, results are shown with r = 4.

3 Results

Figure 2a–c shows mIP SWI obtained using from sensitivity estimated from GRAPPA reconstructed images, sensitivity from ACS data and ESPIRiT-based sensitivity,

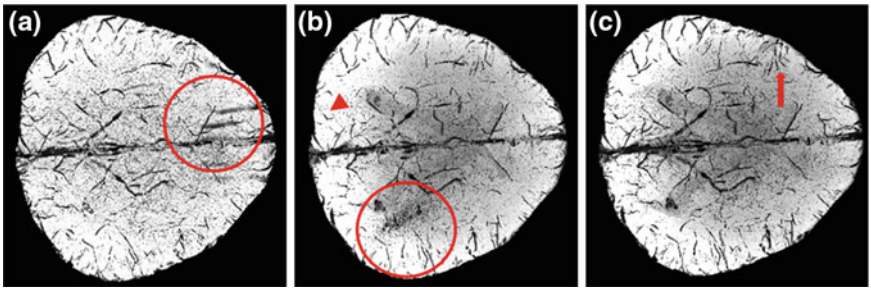

Fig. 2 mIP SWI image obtained after combining the channel images using coil sensitivity estimated from **a** reconstructed coil images. **b** ACS. **c** ESPIRiT sensitivity

respectively. GRAPPA reconstruction was performed on undersampled data with an acceleration of R = 3. From visual inspection, it is observed that combing the channel information using sensitivity estimated from GRAPPA reconstructed images in 2a is highly subjected to streaking artefacts and background noise. The streaks are highlighted using red circles. The reconstruction in 2b is comparatively less noisy. However, small vessels (see arrows) are not detected. ESPIRiT reconstruction in 2c detects more vessels (bold red arrow). Furthermore, background noise appearance is also minimal.

The effect of sensitivity in channel combination is shown using patient data with multiple microbleeds mainly in the left temporal region (Dataset-2). Figure 3 shows the mIP over 16.8 mm (8 slices) of the magnitude SWI obtained after GRAPPA reconstruction with R = 2. Left to right panel shows channel combined image using sensitivity estimated from a GRAPPA reconstructed images, b ACS and c ESPIRiT-based sensitivity, respectively. From the figure, it is observed that mIP SWI images obtained from combined channel images with ESPIRiT sensitivity show better SWI blooming and susceptibility-related contrast. Yellow arrows are used to highlight the better delineation of microbleed when the sensitivity is estimated from ESPIRiT. Red arrows are used to point out the improved resolution in venous structures when the channel combination weights are estimated from dominant eigenvectors of the calibration matrix.

Figure 4 shows the mIP over 9.6 mm (4 slices) of magnitude SWI images of a patient with bleeding in the left frontoparietal convexity (Dataset-3). a–c shows the channel combined image using sensitivity estimated from GRAPPA reconstructed images, centre k-space data and ESPIRiT-based sensitivity, respectively. SWI blooming is observed to be better in panel c compared to both a and b. Red arrows are used to highlight the improvement in venous contrast of the mIP SWI image using ESPIRiT-based sensitivity for channel combination. Even though the superficial veins are visible in panel a and b, better delineation and contrast are accomplished with chan-

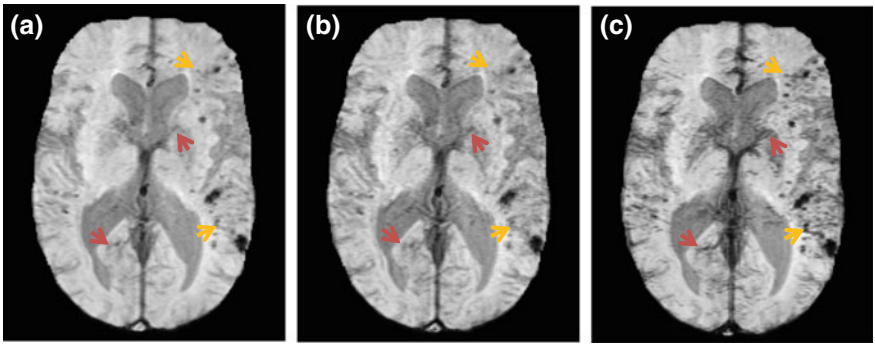

Fig. 3 Reconstructed mIP images from Dataset-2 using sensitivity estimated from **a** reconstructed coil images **b** ACS. **c** ESPIRiT sensitivity. Red arrows are used to indicate the improvement in resolution of faint venous structures and yellow arrows highlight the blooming due to microbleeds in the coil combined image with sensitivity estimated from ESPIRiT

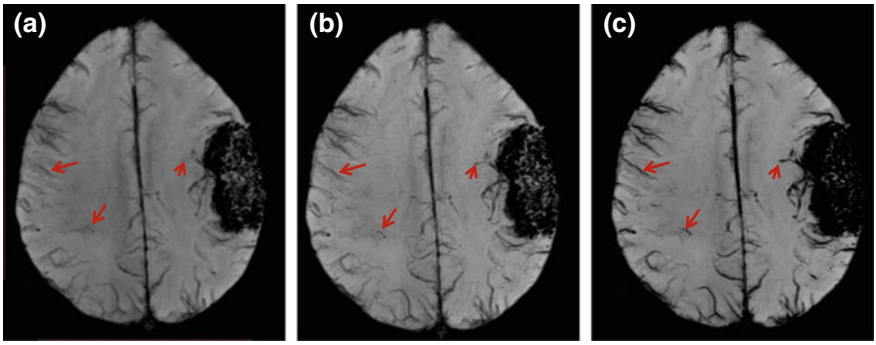

Fig. 4 Reconstructed mIP images from Dataset-3 using sensitivity estimated from **a** reconstructed coil images **b** ACS. **c** ESPIRiT sensitivity. Red arrows indicate the clear visualization of venous structures in panel (**c**)

nel combination using the high-quality sensitivity maps estimated from the SVD of the calibration matrix.

4 Discussion

In recent years, several methods for combining the channel images from array coils have been proposed based on computational requirement and the properties of the combined image. The most common and computationally less intense method for combining the multichannel phase data is the Roemer's method which requires an additional scan with a volume reference coil such as body coil to estimate the coil sensitivity map. The quality of the phase image is directly related to the quality of the sensitivity map used. Improper selection of the sensitivity map may cause phase artefacts and signal loss in the channel combined image. So the main aim of every channel combination method is to develop an SNR optimal coil combination method that retrieves the relative change in a local magnetic field which is related to the local phase change without any additional measurements or scanning.

Three methods have been presented for generating the sensitivity map for combining channel images with array coils. Neither of these methods requires an additional scan. The first method generates the sensitivity after reconstructing the channel images using GRAPPA. The second and third methods do not require the reconstructed channel images for generating the sensitivity map, but they use the autocalibration lines. In the first method, since the sensitivity maps are generated using the reconstructed channel image, noise amplification from GRAPPA causes error in the channel combined image. This effect becomes more critical when a higher acceleration factor is used.

In the second method, the coil sensitivities are generated from centre k-space data which contains the low-frequency component of the channel image together with

some noise components. These noise components may affect the quality of the channel combined image especially when more importance is given to the visualization of finer vascular structures as in SWI. So it is important to suppress the noise component in the sensitivity map. This points to the need for estimating the sensitivity map with high precision. So a well-established method like ESPIRiT can be used to estimate the sensitivity maps from the calibration data which is fully sampled. The sensitivity maps estimated from the dominant eigenvectors of the subspace spanned by the row space of calibration matrix is suitable for combining the coil information with high frequency phase variations as in SWI. Moreover, by using the principle of SVD and choosing the dominant eigenvector of calibration matrix, sensitivity estimation can be made noise-free when compared to that of estimating the sensitivity directly from centre k-space region.

Combination of channel images effectively by preserving the phase variation and reduce the phase artefacts will be beneficial for higher resolution gradient echo scan. Potential of this channel combination method is that it can be used for improving the relative phase change between different ROIs and creating susceptibility maps. With proper background suppression in the channel combined phase image of SWI/SWAN acquisition, quantification of iron deposition in patients with Alzheimer's and Parkinson's can be made robust and reliable.

5 Conclusion

We have evaluated the three methods for generating the sensitivity map for combining channel images from multichannel phased array coils. Neither of these methods requires additional measurements or a volume reference coil making the methods suitable for all field strength. Among the three methods, sensitivity estimated using the dominant eigenvector mentioned as ESPIRiT-based sensitivity in the article shows superior performance over the other two in terms of its ability to preserve the local phase variation and reduction in noise amplification. mIP SWI maps shown the superiority of ESPIRiT-based sensitivity to that achieved with sensitivity estimated from the reconstructed images and centre k-space data.

Acknowledgements The authors are thankful to the Council of Scientific and Industrial Research-Senior Research Fellowship (CSIR-SRF, File No: 09/1208(0001)/2018.EMR-I) and planning board of Govt. of Kerala (GO(Rt) No. 101/2017/ITD.GOK(02/05/2017)), for financial assistance.

References

1. Haacke, E.M., Xu, Y., Cheng, Y.C., Reichenbach, J.R.: Susceptibility weighted imaging (SWI). Magn. Reson. Med. **52**(3), 612–618 (2004)

2. Wycliffe, N.D., Choe, J., Holshouser, B., Oyoyo, U.E., Haacke, E.M., Kido, D.K.: Reliability in detection of hemorrhage in acute stroke by a new three-dimensional gradient recalled echo susceptibility-weighted imaging technique compared to computed tomography: a retrospective study. J. Magn. Reson. Imaging **20**(3), 372–377 (2004)
3. Sehgal, V., Delproposto, Z., Haacke, E.M., Tong, K.A., Wycliffe, N., Kido, D.K., Xu, Y., Neelavalli, J., Haddar, D., Reichenbach, J.R.: Clinical applications of neuroimaging with susceptibility-weighted imaging. J. Magn. Reson. Imaging **22**(4), 439–450 (2005)
4. Haacke, E.M., Cheng, N.Y., House, M.J., Liu, Q., Neelavalli, J., Ogg, R.J., Khan, A., Ayaz, M., Kirsch, W., Obenaus, A.: Imaging iron stores in the brain using magnetic resonance imaging. Magn. Reson. Imaging **23**(1), 1–25 (2005)
5. Sehgal, V., Delproposto, Z., Haddar, D., Haacke, E.M., Sloan, A.E., Zamorano, L.J., Barger, G., Hu, J., Xu, Y., Prabhakaran, K.P., Elangovan, I.R.: Susceptibility-weighted imaging to visualize blood products and improve tumor contrast in the study of brain masses. J. Magn. Reson. Imaging **24**(1), 41–51 (2006)
6. Haacke, E., Makki, M.I., Selvan, M., Latif, Z., Garbern, J., Hu, J., Law, M., Ge, Y.: Susceptibility weighted imaging reveals unique information in multiple-sclerosis lesions using high-field MRI. In: Proceedings of International Society for Magnetic Resonance in Medicine, vol. 15, p. 2302 (2007)
7. Tong, K.A., Ashwal, S., Obenaus, A., Nickerson, J.P., Kido, D., Haacke, E.M.: Susceptibility-weighted MR imaging: a review of clinical applications in children. Am. J. Neuroradiol. **29**(1), 9–17 (2008)
8. Roh, K., Kang, H., Kim, I.: Clinical applications of neuroimaging with susceptibility weighted imaging. J. Korean Soc. Magn. Reson. Med. **18**(4), 290–302 (2014)
9. Haacke, E.M., Mittal, S., Wu, Z., Neelavalli, J., Cheng, Y.C.: Susceptibility-weighted imaging: technical aspects and clinical applications, part 1. Am. J. Neuroradiol. **30**(1), 19–30 (2009)
10. Wang, Y., Yu, Y., Li, D., Bae, K.T., Brown, J.J., Lin, W., Haacke, E.M.: Artery and vein separation using susceptibility-dependent phase in contrast-enhanced MRA. J. Magn. Reson. Imaging **12**(5), 661–670 (2000)
11. Pruessmann, K.P., Weiger, M., Scheidegger, M.B., Boesiger, P.: SENSE: sensitivity encoding for fast MRI. Magn. Reson. Med. **42**(5), 952–962 (1999)
12. Griswold, M.A., Jakob, P.M., Heidemann, R.M., Nittka, M., Jellus, V., Wang, J., Kiefer, B., Haase, A.: Generalized autocalibrating partially parallel acquisitions (GRAPPA). Magn. Reson. Med. **47**(6), 1202–1210 (2002)
13. Wang, Z., Wang, J., Detre, J.A.: Improved data reconstruction method for GRAPPA. Magn. Reson. Med. **54**(3), 738–742 (2005)
14. Lupo, J.M., Banerjee, S., Kelley, D., Xu, D., Vigneron, D.B., Majumdar, S., Nelson, S.J.: Partially-parallel, susceptibility-weighted MR imaging of brain vasculature at 7 Tesla using sensitivity encoding and an autocalibrating parallel technique. In: 28th Annual International Conference of the IEEE Engineering in Medicine and Biology Society, 2006. EMBS'06, pp. 747–750 (2006)
15. Roemer, P.B., Edelstein, W.A., Hayes, C.E., Souza, S.P., Mueller, O.M.: The NMR phased array. Magn. Reson. Med. **16**(2), 192–225 (1990)
16. Uecker, M., Lai, P., Murphy, M.J., Virtue, P., Elad, M., Pauly, J.M., Vasanawala, S.S., Lustig, M.: ESPIRiT—an eigenvalue approach to autocalibrating parallel MRI: where SENSE meets GRAPPA. Magn. Reson. Med. **71**(3), 990–1001 (2014)
17. Horn, R. A., Johnson, C. R.: Matrix analysis. Cambridge University Press (1985)
18. Abduljalil, A.M., Schmalbrock, P., Novak, V., Chakeres, D.W.: Enhanced gray and white matter contrast of phase susceptibility-weighted images in ultra-high-field magnetic resonance imaging. J. Magn. Reson. Imaging **18**(3), 284–290 (2003)